Submitted to Nuclear Physics B

UCRL-19408
Preprint

c.2

ANTIHYPERON AND ANTIPROTON PRODUCTION IN $K^+ p$ INTERACTIONS AT 9 GeV/c

D. Lissauer, G. Alexander, A. Firestone, and G. Goldhaber

November 17, 1969

AEC Contract No. W-7405-eng-48

LAWRENCE RADIATION LABORATORY
UNIVERSITY of CALIFORNIA BERKELEY

UCRL-19408

DISCLAIMER

UCRL-19408

ANTIHYPERON AND ANTIPROTON PRODUCTION IN K^+p INTERACTIONS AT 9 GeV/c[†]

D. Lissauer, G. Alexander,[‡] A. Firestone, and G. Goldhaber

Department of Physics and Lawrence Radiation Laboratory
University of California, Berkeley, California 94720

November 17, 1969

ABSTRACT

We have analyzed the reactions of the type $K^+p \to \bar{Y}NN(\pi)$ in K^+p interactions at 9 GeV/c, where $\bar{Y}$ refers to a $\bar{\Lambda}$ or $\bar{\Sigma}$ antihyperon. We have also studied the production of $\bar{\Xi}^-$ in the reaction $K^+p \to \bar{\Xi}^-YN(\pi)$ and of antiprotons in the reaction $K^+p \to K^+p\bar{p}p$. With twice the data previously reported we observe again a low mass enhancement in the $\bar{\Lambda}N$ final state and also observe some indications of a similar enhancement in the non-exotic $\bar{\Sigma}^{\pm}N$ final states. This enhancement has the quantum numbers of an $I = 1/2$ K^* resonance with mass $M = 2240 \pm 20$ MeV and width $\Gamma = 80 \pm 20$ MeV.

[†]Work supported by the U. S. Atomic Energy Commission.

[‡]Permanent address: Department of Physics, Tel-Aviv University, Tel-Aviv, Israel.

1. INTRODUCTION

In the present paper we present the final analysis of our data on anti-hyperon and antiproton production in K^+p interactions at 9 GeV/c[1]. Preliminary results on some of the final states and the experimental procedures used have been described in the literature[2,3].

The study of the $\bar{Y}N$ final state affords the opportunity to study possible higher mass K^* resonances, which may not appear distinctly in the $K^+ + m\pi$ ($m \geq 1$) decay modes due to the large backgrounds present. Furthermore, evidence for $N\bar{N}$ decay of higher mass nonstrange mesons has been reported[4], and similar decays of higher mass K^* resonances into $\bar{Y}N$ is thus expected to occur. In addition, arguments have been given for the existence of exotic boson resonances which might decay primarily into baryon-antibaryon final states[5].

2. EXPERIMENTAL

The present study was carried out on ~ 200,000 pictures taken with the 80-inch hydrogen bubble chamber at the Brookhaven National Laboratory AGS, which was exposed to an rf-separated 9-GeV/c K^+ beam. Events having a visible V^o decay were measured with the LRL Flying Spot Digitizer. Remeasures and events having at least one charged decay were digitized on a conventional measuring machine. The events were spatially reconstructed and kinematically fitted in the program SIOUX.

All events kinematically consistent with at least one antilambda production fit were examined on the scan table by a physicist to check ionization consistency and to resolve kinematic ambiguities. All events kinematically consistent with the three constraint antilambda decay fit but not kinematically consistent with any antilambda production fit were remeasured. This procedure was repeated three times to correct for failures due to measurement errors.

Of the 306 events in the complete sample kinematically consistent with at least one antilambda production fit, 102 events were also kinematically consistent with the three constraint K^o decay fit. A total of 57 of these events were either judged on the scan table to be K^o decays or remained ambiguous and were not included in this sample. All events kinematically consistent with a charged antisigma or charged anticascade decay were examined on the scan table by a physicist and only those events uniquely determined by ionization consistency as antisigma or anticascade events were included in this sample. Although this procedure is necessary to obtain a pure sample of $\overline{\Sigma^{\pm}}$ and $\overline{\Xi^-}$ events, it does reject some real $\overline{\Sigma^{\pm}}$ and $\overline{\Xi^-}$ events which results in an underestimate of the cross sections involved. It is for this reason that the cross sections for the $\overline{\Sigma^{\pm}}$ and $\overline{\Xi^-}$ states quoted in Table 1 are presented as lower limits. The four-constraint, four-pronged reaction, $K^+p \rightarrow K^+\bar{p}pp$ is identified unambiguously by kinematics and scan table ionization. Table 1 lists the number of events identified in each final state and its corresponding cross section. The cross sections quoted have been corrected both for decay in neutral modes and escape probability. The errors quoted are purely statistical.

3. ANTILAMBDA PRODUCTION

The three constraints of the $\bar{\Lambda} \rightarrow \bar{p}\pi^+$ decay fit; coplanarity, transverse momentum balance, and invariant mass, in addition to the identification of the antiproton on the scan table by ionization measurement, serve to identify the antilambda decays unambiguously. The measured lifetime of the complete sample of 245 $\bar{\Lambda}$ decays is $2.42 \pm 0.20 \times 10^{-10}$ sec in good agreement with the value quoted in the Particle Data Tables for the Λ hyperon[6]. Of the 55 events

listed in Table 1 as $\bar{\Lambda}pp + \overline{\Sigma^o}pp$, 28 events were kinematically ambiguous between the seven-constraint multivertex interpretation $\bar{\Lambda}pp$ and the five-constraint multivertex interpretation $\overline{\Sigma^o}pp$. A total of 23 events were identified unambiguously as $\bar{\Lambda}pp$ and 4 events as $\overline{\Sigma^o}pp$. In our sample, the events ambiguous between a $\overline{\Sigma^o}$ or $\bar{\Lambda}$ interpretation show a backward peaked angular distribution for the γ in the $\overline{\Sigma^o}$ center of mass, while real $\overline{\Sigma^o} \rightarrow \gamma\bar{\Lambda}$ decay would have an isotropic γ angular distribution in the $\overline{\Sigma^o}$ center of mass. We have also investigated the ambiguity by Monte-Carlo techniques, and found that a real $\overline{\Sigma^o}$ event rarely fits a $\bar{\Lambda}$ hypothesis but that a real $\bar{\Lambda}$ will easily fit a less constrained $\overline{\Sigma^o}$ hypothesis. Thus we believe that all our ambiguous events are in fact $\bar{\Lambda}$ events, and for brevity refer to the combined $\bar{\Lambda}pp$ and $\overline{\Sigma^o}pp$ sample simply as $\bar{\Lambda}pp$, but note the presence of a $\sim 7\%$ $\overline{\Sigma^o}pp$ contamination. The four-body final states $\overline{\Sigma^o}pp\pi^o$ and $\overline{\Sigma^o}pn\pi^+$ are underconstrained and therefore could not be identified in this experiment. We cannot, however, rule out the possibility that a fraction of the events which fit $\bar{\Lambda}pp\pi^o$ or $\bar{\Lambda}pn\pi^+$ are in fact the corresponding $\overline{\Sigma^o}$ fit.

In order to study the $\bar{\Lambda}N$ system we first examine the production mechanism of the three final states $\bar{\Lambda}pp$, $\bar{\Lambda}pp\pi^o$, and $\bar{\Lambda}pn\pi^+$. Figure 1 shows the center-of-mass angular correlations of the nucleons in these three final states. The $\bar{\Lambda}pp$ events are highly peripheral with one proton emitted forward in the production center of mass ($\cos\theta_p > 0$) and the other emitted backward ($\cos\theta_p < 0$). The nucleons in the $\bar{\Lambda}pp\pi^o$ and $\bar{\Lambda}pn\pi^+$ events show a similar strong peripheral signal but in these cases there is also some nonperipheral background. The $\bar{\Lambda}$ angular distributions in the production center of mass are shown in Fig. 2a, b, and c. In these final states the $\bar{\Lambda}$ is peaked in the forward direction. In both $\bar{\Lambda}pp\pi^o$ and $\bar{\Lambda}pn\pi^+$ final states, the pion angular distribution in the center of mass (Fig. 2d) shows only a small forward peak above a largely isotropic distribution.

In view of the highly peripheral nature of the large majority of the events, it is reasonable to assume that a nucleon-antihyperon pair is produced at the incident K^+ vertex, the nucleon backward in the production center of

mass is produced at the target vertex, and that the production mechanism is dominated by Pomeranchuk or nonstrange meson exchange. For events with an additional pion it is not clear, from the present data, at which vertex the pion is to be assigned in such an exchange diagram.

In Fig. 3 we plot the antihyperon-pion and baryon-pion mass distributions for the four-body final states $\bar{\Lambda}pp\pi^o$ and $\bar{\Lambda}pn\pi^+$. There is no clear evidence for the $\bar{\Lambda}\pi$ decay of the $\overline{Y^*_{1385}}$ in Fig. 3a and 3b, and we observe only a weak Δ^{++}_{1236} signal in Fig. 3c, a weak Δ^{+}_{1236} signal in Fig. 3d, but none in Fig. 3e. The $\bar{\Lambda}N\pi$ mass distributions (not shown) do not show significant structure in any of the three charge combinations. Thus in the four-body events, the pion does not appear to be strongly associated with any of the other particles. To exploit the peripheral features of the data we impose a peripheral cut on the events, i.e., we select only those events in which one nucleon is forward in the production center of mass ($\cos\theta_N > 0$) and the other nucleon is backward ($\cos\theta_N < 0$). This peripheral cut selects a total of 183 events in the three final states $\bar{\Lambda}pp$ (52), $\bar{\Lambda}pp\pi^o$ (28), $\bar{\Lambda}pn\pi^+$ (103).

In Fig. 4 we show the Dalitz plot for the $\bar{\Lambda}pp$ events, $M^2(\bar{\Lambda}p_f)$ vs $M^2(\bar{\Lambda}p_b)$. There is a clear concentration of events in the low $M^2(\bar{\Lambda}p_f)$ region. In Fig. 5 we show the projection $M^2(\bar{\Lambda}p_f)$. In Fig. 6a we plot the $\bar{\Lambda}$-nucleon mass distribution for all 237 events in the final states $\bar{\Lambda}pp$, $\bar{\Lambda}pp\pi^o$, and $\bar{\Lambda}pn\pi^+$, with two mass combinations plotted per event. In Fig. 6b we plot the same mass distribution for the 183 peripheral events where only the forward nucleon mass combination is plotted. In both cases we observe a strong low-mass $\bar{\Lambda}N$ enhancement, but from the present sample we cannot ascertain with certainty the nature of this enhancement. If we interpret it as a K^* resonance, the best parameters corresponding to a Breit-Wigner shape are found to be $M = 2240\pm20$ MeV and $\Gamma = 80\pm20$ MeV with $40\pm10\%$ resonance production.

To further explore the $\bar{\Lambda}N$ mass enhancement region (2.20 to 2.28 GeV) we have studied the decay angular distribution of this system as well as the $\bar{\Lambda}$ polarization. In Fig. 7 we show the distribution in the decay angle of the $\bar{\Lambda}N_f$ system in the $\bar{\Lambda}N_f$ rest frame (Jackson angle)[7]) with α defined as the angle between the incident K^+ and the $\bar{\Lambda}$ for events in the enhancement region (Fig. 7a), and in two 40-MeV bands on either side of the enhancement (background Fig. 7b). The distribution in cos α is strongly backward peaked outside the enhancement region while it is consistent with an isotropic distribution (after subtraction of background, see Fig. 7c) inside the enhancement region. The distribution in ϕ (Treiman-Yang angle) reveals no strong distinguishing features (not shown). The polarization of the $\bar{\Lambda}$ along the normal to the production plane of the $\bar{\Lambda}N_f$ system was calculated from the decay direction using the value $\alpha(\bar{\Lambda}) = -\alpha(\Lambda) = -0.64$ for the decay parameter α[6]). We find the polarization to be 0.45 ± 0.20 in the "enhancement region" and -0.002 ± 0.11 outside this region. Figure 8 shows the polarization as a function of the $\bar{\Lambda}N_f$ mass. The only indication for nonzero polarization is in the enhancement region.

If the enhancement in the $\bar{\Lambda}N$ mass is to be interpreted as a $K^* \rightarrow \bar{\Lambda}N$ resonance decay its isotopic spin would be 1/2. An isotopic spin value of 3/2 is possible only if the $\bar{\Lambda}$-antihyperons in the enhancement region are in fact the decay products of $\bar{\Sigma}^0$-antihyperons, but this is not the case as was shown previously[2]).

4. ANTISIGMA PRODUCTION

In order to ascertain the reliability of our sample of charged $\bar{\Sigma}$ events we have calculated the lifetimes of the $\bar{\Sigma}^+$, $\bar{\Sigma}^-$ using the maximum likelihood method, and have found them to be $\tau(\bar{\Sigma}^-) = 1.4^{+0.28}_{-0.20} \times 10^{-10}$ sec, and $\tau(\bar{\Sigma}^+) =$

$0.92^{+0.3}_{-0.17} \times 10^{-10}$ sec which are consistent with the lifetimes given in the Particle Data Tables for the Σ^- and Σ^+ hyperons respectively[6].

To study the nature of events with $\overline{\Sigma^{\pm}}$ production we examined the seven final states $\overline{\Sigma^-}pn$, $\overline{\Sigma^-}pp\pi^-$, $\overline{\Sigma^-}pp\pi\pi^o$, $\overline{\Sigma^-}pn\pi^+\pi^+$, $\overline{\Sigma^+}pp\pi^+\pi^o$, $\overline{\Sigma^+}pp\pi^+$, and $\overline{\Sigma^+}pn\pi^+\pi^+$. Figure 9 shows the angular distributions of the nucleons and $\overline{\Sigma^{\pm}}$ in the production center of mass. We note that in all cases the nucleons are both forward and backward peaked, and that the $\overline{\Sigma^{\pm}}$ shows similar behavior. We further note that the forward and backward peaks for the $\overline{\Sigma^{\pm}}$-antihyperons are approximately equal in magnitude. If we assume the reaction proceeds via peripheral diagrams with single particle exchange then the forward $\overline{\Sigma}$-antihyperons are most likely produced in a diagram such as that shown in Fig. 10a while the backward $\overline{\Sigma}$-antihyperons are most likely produced by a diagram such as that shown in Fig. 10b. Figure 10a could include Pomeranchuk exchange, π, or ρ exchange while that in Fig. 10b involves Y or Y^* exchange. A priori one would expect Fig. 10a to dominate this reaction at high energies but it appears that both diagrams contribute about equally in this experiment.

In Fig. 11 we plot the mass distributions of the charged $\overline{\Sigma^{\pm}}N$ system. Figure 11d shows the $(\overline{\Sigma}N)$ mass distribution for all $\overline{\Sigma}$ reactions and a clear low mass enhancement is seen at a mass of $M = 2240 \pm 20$ MeV. The shaded distribution in Fig. 11d shows the $\overline{\Sigma}N$ mass for only those charge combinations which cannot belong to an SU_3 octet or singlet (exotic mesons). The low mass enhancement clearly goes with the non-exotic contribution. In Fig. 12 we show the $\overline{Y}N$ mass distribution for all the $\overline{\Lambda}N$ and $\overline{\Sigma}N$ charge combinations which are non-exotic and with the peripheral cut described. The enhancement at $M = 2240$ MeV is very prominent in this combined spectrum. We point out that this enhancement is not at threshold but is centered about 200 MeV above $\overline{\Lambda}N$ threshold. We have tried to fit the $\overline{Y}N$ mass distribution to various peripheral

models. All such attempts were unsuccessful because the high degree of peripheralism required to reproduce the observed narrow width of the peak is inconsistent with the observed t-distribution ($\frac{d\sigma}{dt} \propto e^{0.7t}$), and also, for the $\bar{\Lambda}$ events, forces the mass peak down to values well below 2240 MeV.

5. ANTIXI PRODUCTION

We have also searched for antihyperons of strangeness equal to or greater than two, specifically $\overline{\Xi^-}$, $\overline{\Omega^-}$. At present we have clearly identified 19 events as exhibiting $\overline{\Xi^-}$ production. No events were found which can be shown to involve $\overline{\Omega^-}$ production. If one event of this type were found, it would correspond to a cross section of 0.13 μb. We have calculated the lifetime of the $\overline{\Xi^-}$ using the maximum likelihood method and found it to be $\tau(\overline{\Xi^-}) = 1.9^{+0.7}_{-0.5} \times 10^{-10}$ sec which is consistent with the values recorded in the Particle Data Tables for the Ξ^- hyperon[6]). In Fig. 13 we show the Dalitz plot $M^2(\bar{\Xi}Y)$ vs $M^2(YN)$ for all 19 $\overline{\Xi^-}$ events. For reactions with missing mass we interpret the missing particle(s) as a hyperon if we see a nucleon, or a nucleon if we see a $\bar{\Lambda}$ or $\overline{\Sigma^\pm}$. With the present statistics we find no indication of any enhancement in either the $\overline{\Xi^-}Y$ or $\overline{\Xi^-}N$ systems. We have also looked at the production angular distributions as well as the correlations between the production angles of the final state particles. With the present statistics there are no noticeable angular correlations, and all angular distributions are consistent with isotropy.

6. ANTIPROTON PRODUCTION

We have studied all the four-constraint four-pronged interactions and have extracted the $K^+\bar{p}pp$ final state. The kinematic constraints for this final state are sufficient to allow complete identification of these events with information on scan table ionization. We have found 38 events of this type which corresponds to a cross section of 3.0±0.5 μb. The angular distribution

of the nucleons in this final state indicate that these events are not very peripheral. In Fig. 14a we show the $\bar{p}p$ mass distribution, which shows indications of an enhancement centered at 2 GeV. Present statistics do not permit a more detailed study of this enhancement. In Figs. 14b and 14c we show the $(K^+\bar{p}p)$ and $(p\bar{p}p)$ mass distributions respectively. No significant structure is observed in either distribution, but we note that the suggested $(p\bar{p}p)$ mass enhancement at 3755 MeV reported earlier[8] lies just above our kinematic limits. In Fig. 14d we show the $(K^+\bar{p})$ mass distribution, but do not observe any significant $\bar{Y}^*$ production.

We thank R. Shutt and the staff of the 80-inch Bubble Chamber and H. Foelsche and the AGS staff for helping with the exposure. We acknowledge the valuable support given by our scanning and programming staff, in particular B. M. Sheldon, D. V. Armstrong, and E. R. Burns.

REFERENCES

1) Studies of $\bar{Y}$ production in K^+p interactions have been previously reported in the literature. See for example: G. Bassompierre et al., Nuovo Cimento 48A (1967) 589; C.-Y. Chien et al., Phys. Letters 25B (1967) 426; J. C. Berlinghieri et al., Phys. Letters 27B (1968) 665; and M. Alston-Garnjost et al., Bull. Am. Phys. Soc. 14 (1969) 560.

2) G. Alexander, A. Firestone, G. Goldhaber, and B. C. Shen, Phys. Rev. Letters 20 (1968) 755.

3) B. C. Shen, A. Firestone, and G. Goldhaber, Phys. Letters 25B (1967) 443.

4) Ch. d'Andlau et al., Nucl. Physics B5 (1968) 693; M. N. Focacci et al., Phys. Rev. Letter 17 (1966) 890; R. J. Abrams et al., Phys. Rev. Letters 18 (1967) 1209; R. Armenteros et al., Phys. Letters 9 (1964) 207; N. Barash et al., Phys. Rev. 145 (1966) 1095; also I. Butterworth, Proceedings of the International Conference on Elementary Particles, Heidelberg 1967, and references therein.

5) J. Rosner, Phys. Rev. Letters 21 (1968) 950.

6) Particle Data Group, Review of Particle Properties, UCRL-8030, Revised January 1969.

7) J. D. Jackson, Nuovo Cimento 34 (1964) 1644.

8) R. Ehrlich et al., Observation of a $p\bar{p}$ (3755) Enhancement in the Reaction $\pi^+p \rightarrow \pi^+pp\bar{p}$ at 8.4 BeV/c, Rutgers preprint (1969).

Table 1. Cross section summary.

Final state	Number of events	Cross section (μb)
$\bar{\Lambda}pp + \bar{\Sigma}^{o}pp$	55	12.8±1.7
$\bar{\Lambda}pp\pi^{o}$	34	7.9±1.3
$\bar{\Lambda}pn\pi^{+}$	148	34.6±2.8
$\bar{\Lambda}pp\pi^{+}\pi^{-}$	12	2.8±0.79
$\bar{\Sigma}^{-}pn$	24	> 1.8
$\bar{\Sigma}^{-}pp\pi^{-}$	10	> 0.76
$\bar{\Sigma}^{-}pp\pi^{-}\pi^{o}$	1	> 0.07
$\bar{\Sigma}^{-}pn\pi^{+}\pi^{-}$	18	> 1.38
$\bar{\Sigma}^{+}pp\pi^{+}$	11	> 0.85
$\bar{\Sigma}^{+}pp\pi^{+}\pi^{o}$	6	> 0.46
$\bar{\Sigma}^{+}pn\pi^{+}\pi^{+}$	2	> 0.15
$\bar{\Xi}^{-}\Lambda^{o}p$	3	> 0.65
$\bar{\Xi}^{-}\Sigma^{o}p$	3	> 0.58
$\bar{\Xi}^{-}mmp$	4	> 0.30
$\bar{\Xi}^{-}\Sigma^{+}n$	4	> 0.30
$\bar{\Xi}^{-}\Sigma^{+}mm$	1	> 0.07
$\bar{\Xi}^{-}\Lambda^{o}n\pi^{+}$	2	> 0.28
$\bar{\Xi}^{-}\Lambda^{o}p\pi^{o}$	2	> 0.31
$K^{+}pp\bar{p}$	38	3.0±0.5

FIGURE CAPTIONS

Fig. 1. Scatter plot of cos θ_N vs cos θ_N for (a) $\bar{\Lambda}pp$ events, (b) $\bar{\Lambda}pn\pi^+$ events, and (c) $\bar{\Lambda}pp\pi^o$ events. The plots in (a) and (c) where there are two identical nucleons have been folded about 45^o.

Fig. 2. Distributions in cos $\theta_{\bar{\Lambda}}$ for (a) $\bar{\Lambda}pn\pi^+$ events, (b) $\bar{\Lambda}pp$ events and (c) $\bar{\Lambda}pp\pi^o$ events. Distribution in cos θ_π for $\bar{\Lambda}pn\pi^+$ and $\bar{\Lambda}pp\pi^o$ events in (d).

Fig. 3. (a) $M(\bar{\Lambda}\pi^o)$ for $\bar{\Lambda}pp\pi^o$ events; (b) $M(\bar{\Lambda}\pi^+)$ for $\bar{\Lambda}pn\pi^+$ events; (c) $M(p\pi^+)$ for $\bar{\Lambda}pn\pi^+$ events; (d) $M(n\pi^+)$ for $\bar{\Lambda}pn\pi^+$ events; and (e) $M(p\pi^o)$ for $\bar{\Lambda}pp\pi^o$ events.

Fig. 4. Dalitz plot for the $\bar{\Lambda}pp$ events. Here p_f is the forward proton and p_b is the backward proton.

Fig. 5. $M^2(\bar{\Lambda}p_f)$ for $\bar{\Lambda}pp$ events.

Fig. 6. (a) $M(\bar{\Lambda}N)$ and (b) $M(\bar{\Lambda}N_f)$ for all $\bar{\Lambda}pp$, $\bar{\Lambda}pn\pi^+$, and $\bar{\Lambda}pp\pi^o$ events.

Fig. 7. Distributions in cos α for (a) enhancement region, (b) background, and (c) subtracted events.

Fig. 8. $\bar{\Lambda}$ polarization as a function of $M(\bar{\Lambda}N_f)$.

Fig. 9. Center-of-mass angular distributions for (a) and (b) $\bar{\Sigma}^+$ events, (c) and (d) four- and five-body $\bar{\Sigma}^-$ events, and (e) and (f) $\bar{\Sigma}pn$ events.

Fig. 10. Possible exchange diagrams for $\bar{\Sigma}$ production with (a) Pomeranchuk or meson exchange, and (b) hyperon exchange.

Fig. 11. $M(\bar{\Sigma}^{\pm}N)$ for (a) $\bar{\Sigma}^-pn$ events, (b) four- and five-body $\bar{\Sigma}^-$ events, (c) $\bar{\Sigma}^+$ events, and (d) all $\bar{\Sigma}$ events. In (d) the shaded region refers to the exotic $(\bar{\Sigma}^{\pm}N)$ combinations.

Fig. 12. $M(\bar{Y}N)$ for all $\bar{\Lambda}N$ and $\bar{\Sigma}N$ non-exotic combinations with the described peripheral cut.

Fig. 13. Dalitz plot for the $\bar{\Xi}^-YN$ events. The boundary for this Dalitz plot has been computed for the reaction $K^+p \rightarrow \bar{\Xi}^-\bar{\Lambda}p$. Thus not all events fall inside this boundary.

Fig. 14. (a) $M(\bar{p}p)$, (b) $M(K^+\bar{p}p)$, (c) $M(pp\bar{p})$, and (d) $M(K^+\bar{p})$ for the $K^+p\bar{p}p$ events.

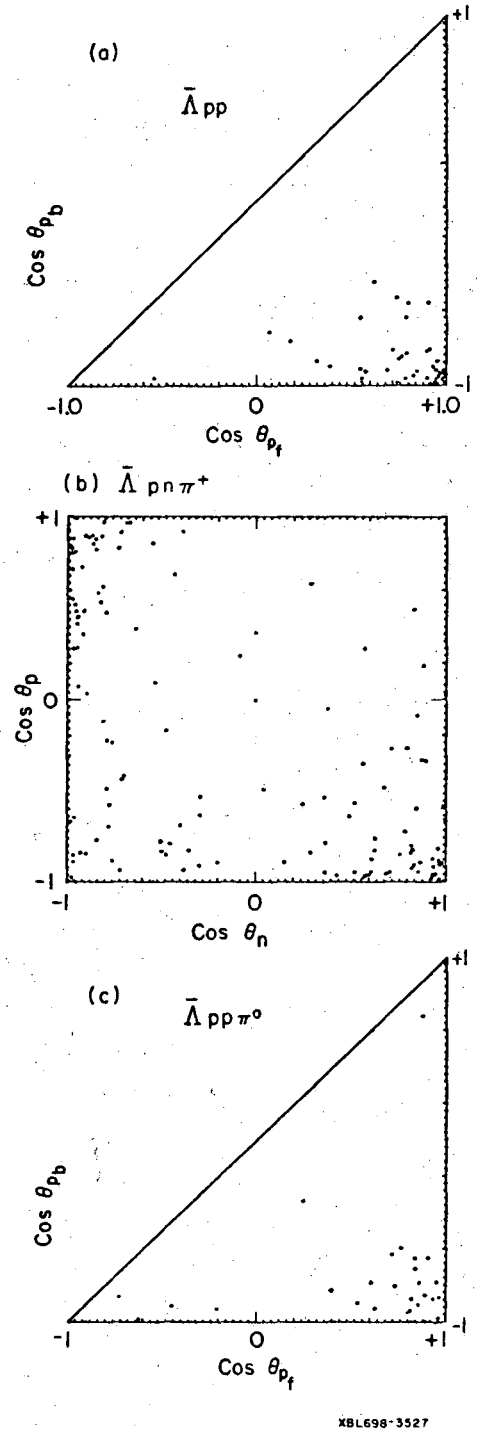
(a)
$\bar{\Lambda}$ pp
Cos θ_{p_b}
+1
-1
-1.0
0
+1.0
Cos θ_{p_f}
(b) $\bar{\Lambda}$ p n π^+
Cos θ_p
+1
0
-1
-1
0
+1
Cos θ_n
(c)
$\bar{\Lambda}$ p p π^o
Cos θ_{p_b}
+1
-1
-1
0
+1
Cos θ_{p_f}
XBL698-3527

Fig. 1

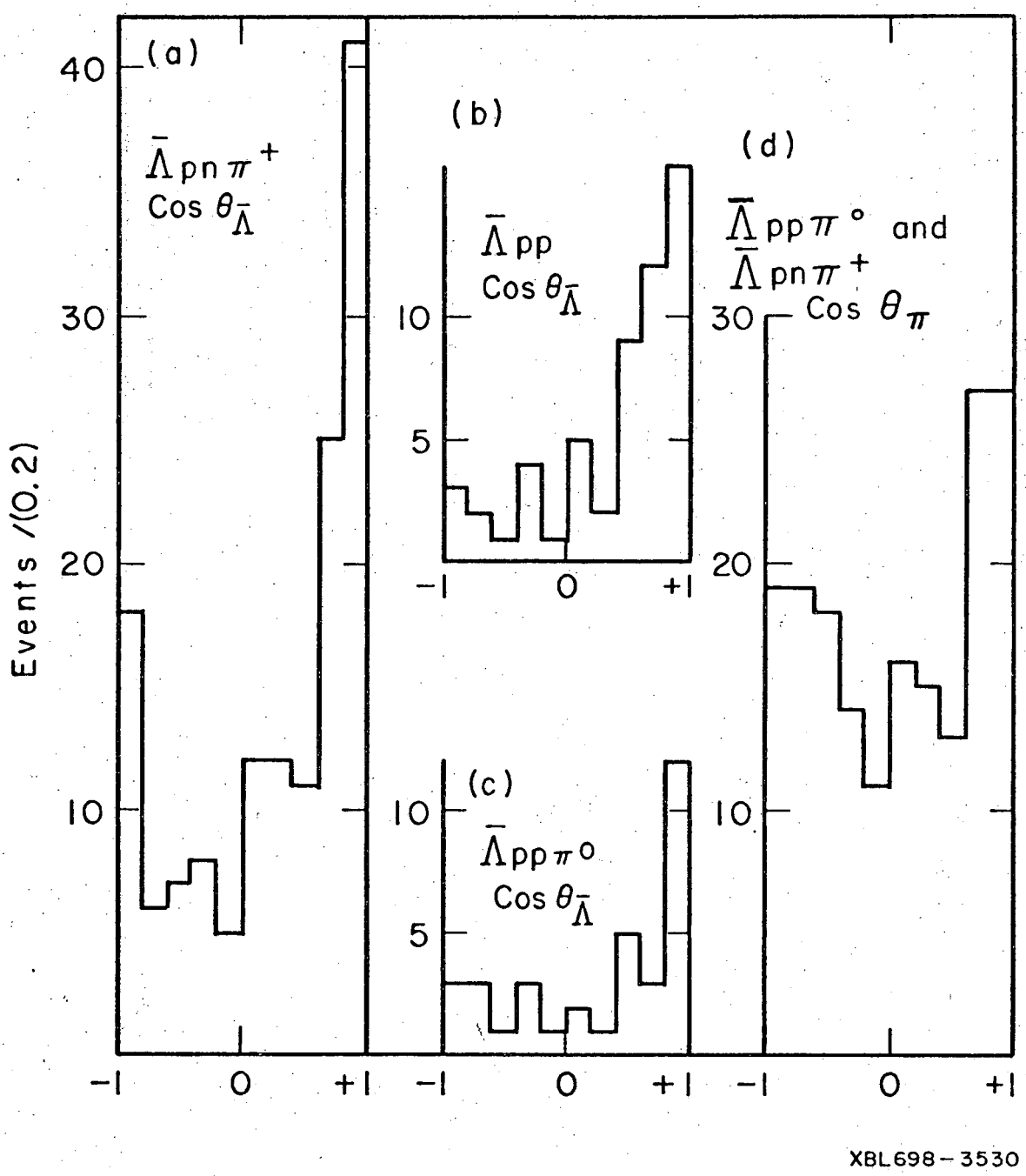
(a)
$\bar{\Lambda}$ pn π^+
Cos $\theta_{\bar{\Lambda}}$
(b)
$\bar{\Lambda}$ pp
Cos $\theta_{\bar{\Lambda}}$
(c)
$\bar{\Lambda}$ pp π^0
Cos $\theta_{\bar{\Lambda}}$
(d)
$\bar{\Lambda}$ pp π^0 and
$\bar{\Lambda}$ pn π^+
Cos θ_{π}
Events /(0.2)
40
30
20
10
5
-1
0
+1
XBL698-3530

Fig. 2

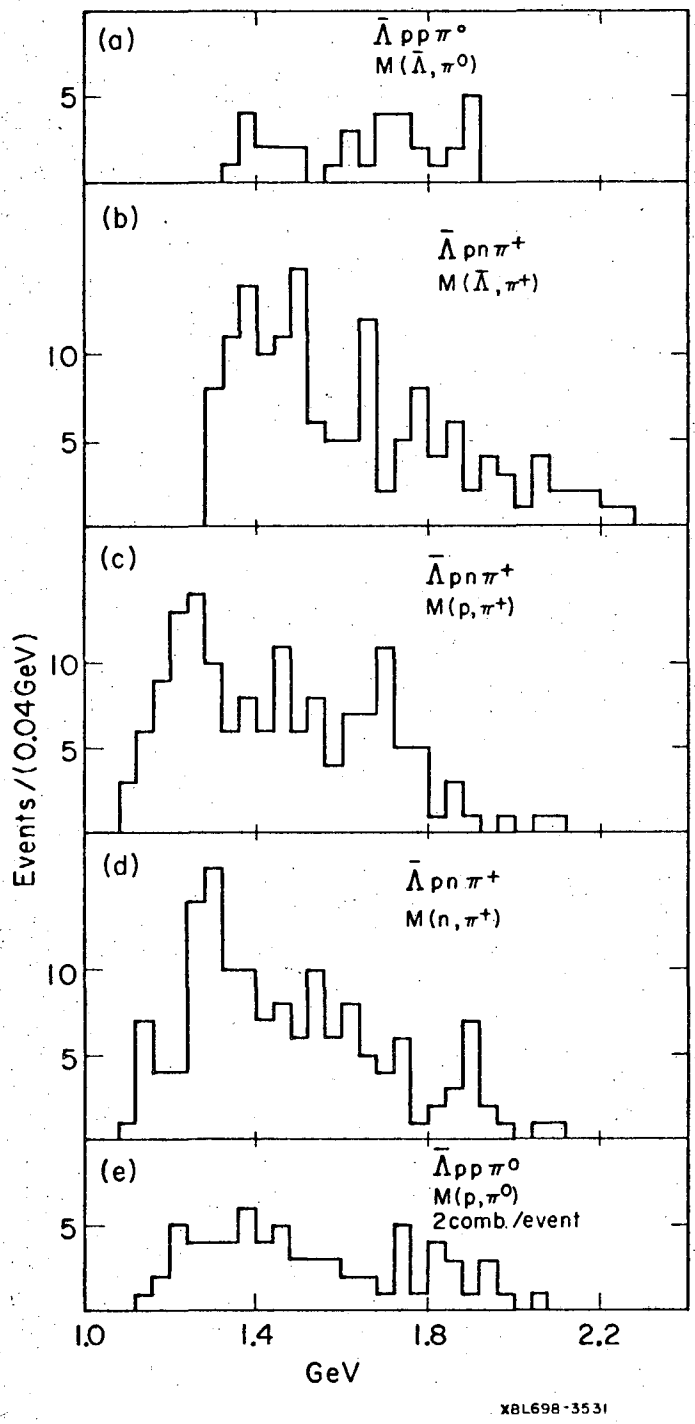
(a)
$\bar{\Lambda}$ pp π^0
M($\bar{\Lambda}$, π^0)
(b)
$\bar{\Lambda}$ pn π^+
M($\bar{\Lambda}$, π^+)
(c)
$\bar{\Lambda}$ pn π^+
M(p, π^+)
(d)
$\bar{\Lambda}$ pn π^+
M(n, π^+)
(e)
$\bar{\Lambda}$ pp π^0
M(p, π^0)
2 comb. /event
Events / (0.04 GeV)
5
10
1.0
1.4
1.8
2.2
GeV
XBL698-3531

Fig. 3

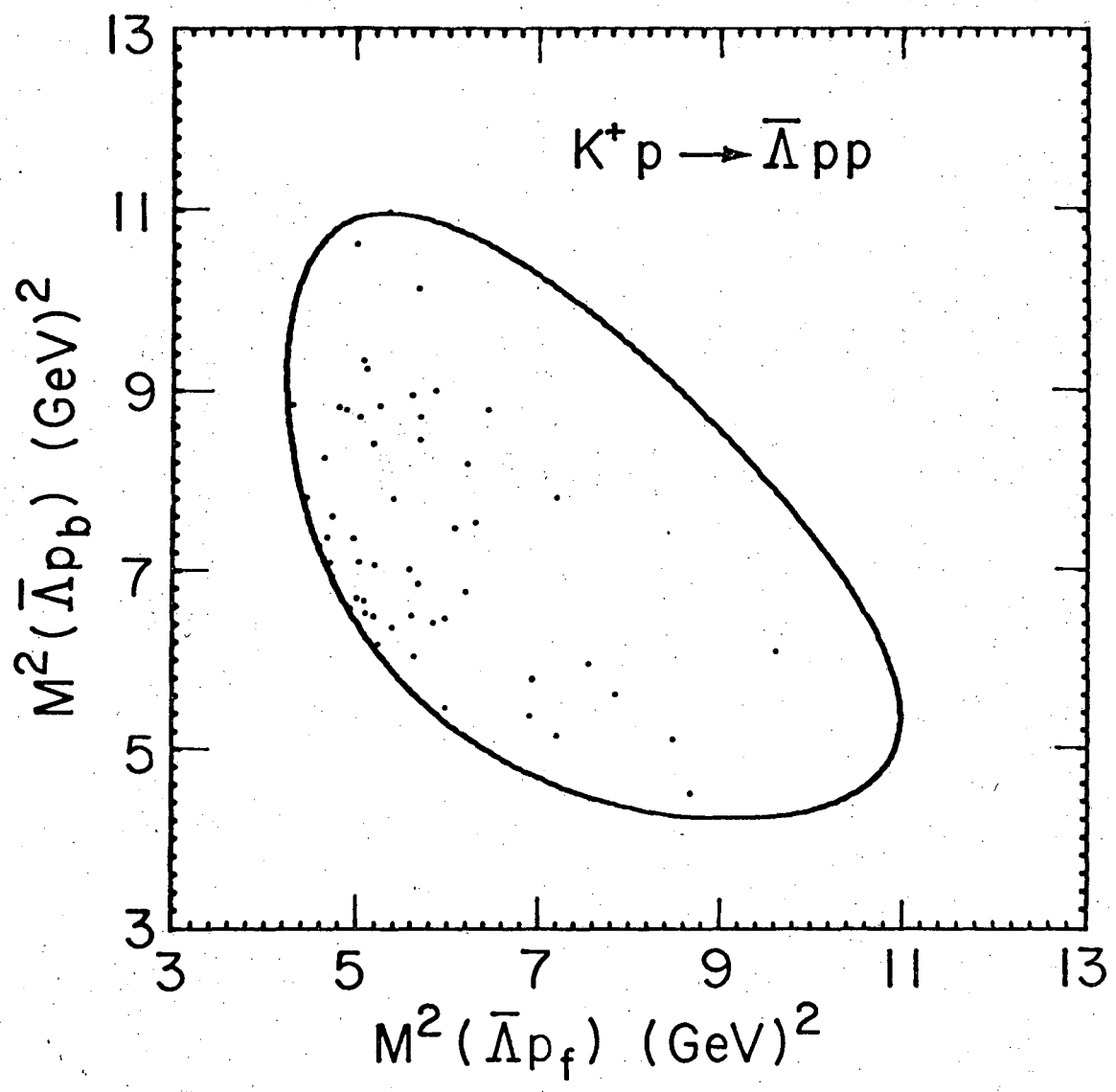

XBL698-3526

Fig. 4

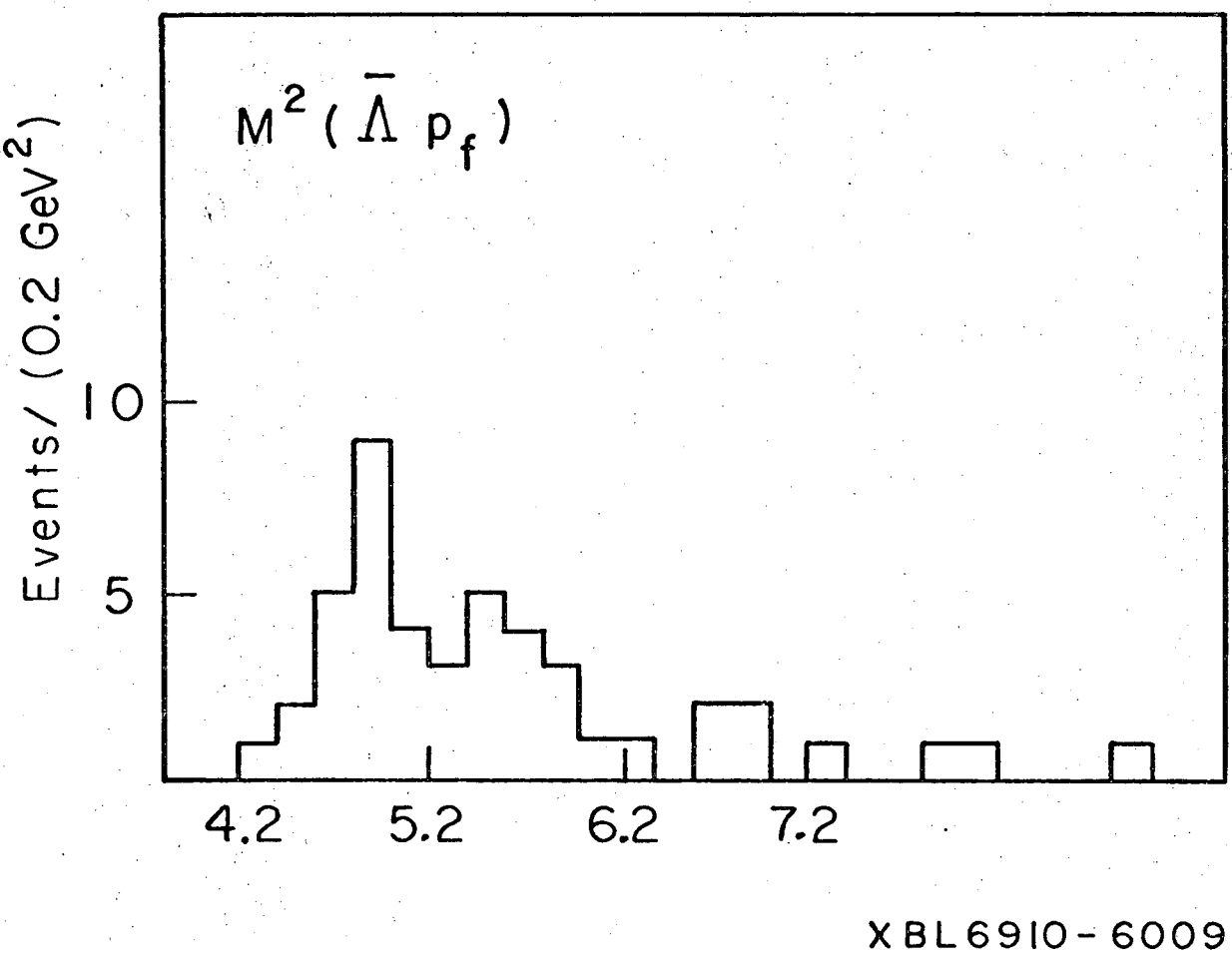

Fig. 5

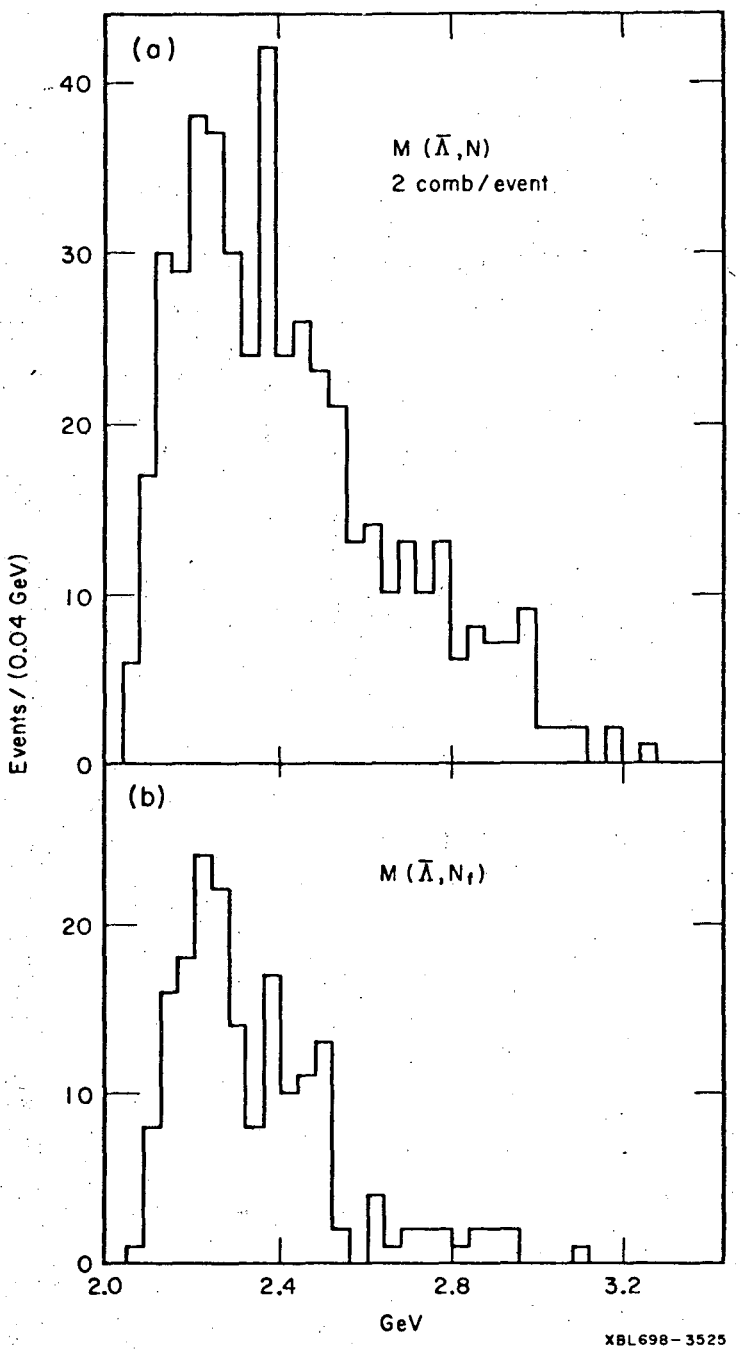
(a)
M (Λ̄,N)
2 comb/event
(b)
M (Λ̄,N_f)
Events/(0.04 GeV)
0
10
20
30
40
2.0
2.4
2.8
3.2
GeV
XBL698-3525

Fig. 6

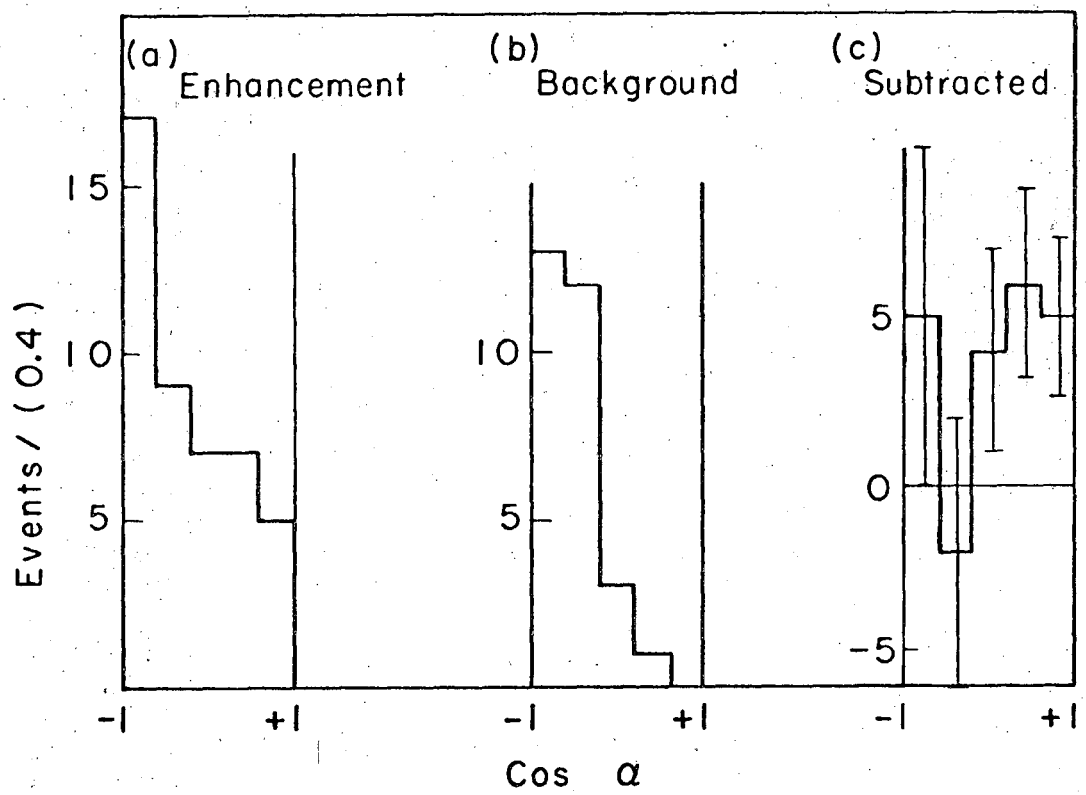
(a)
Enhancement
(b)
Background
(c)
Subtracted
Events / (0.4)
15
10
5
10
5
5
0
-5
-1
+1
-1
+1
-1
+1
Cos α
XBL6910-6004

Fig. 7

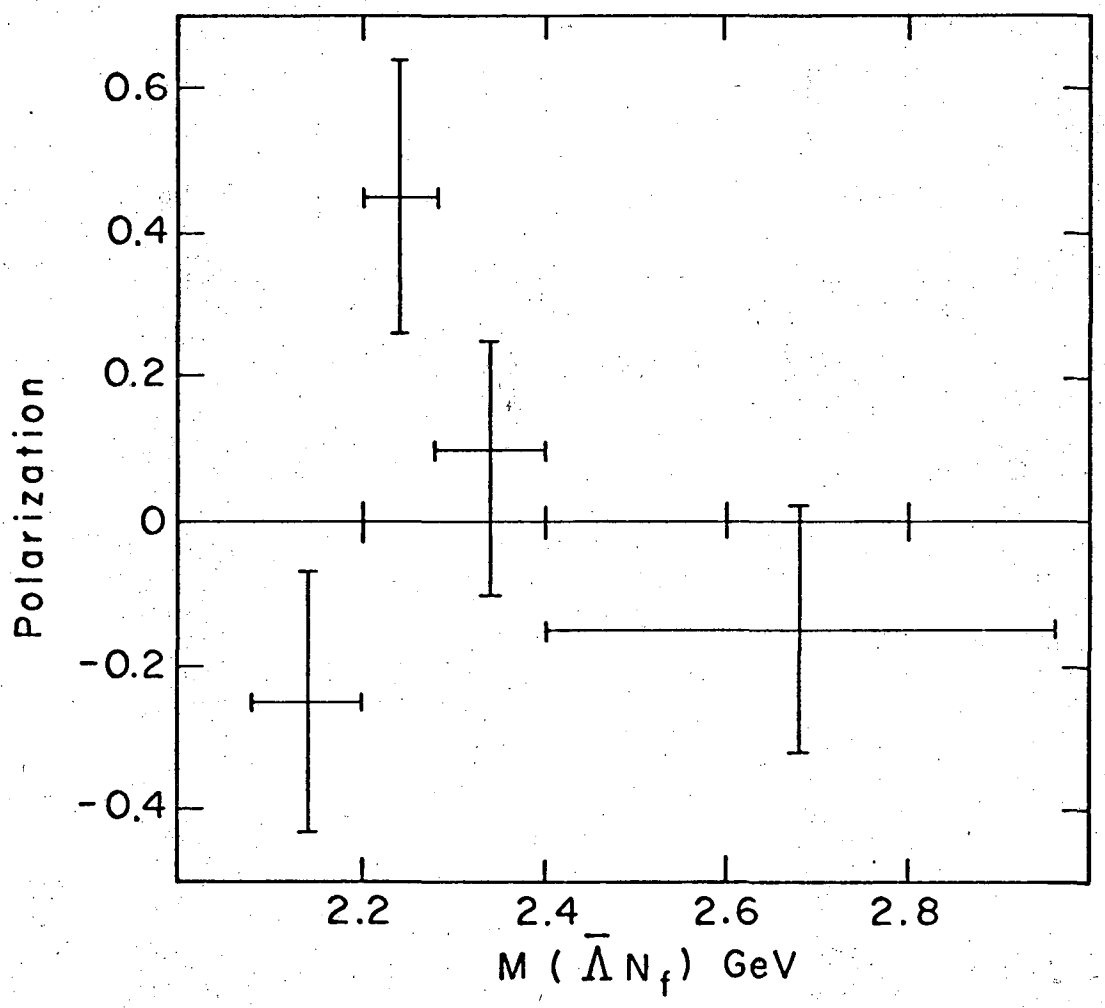

XBL6910-6007

Fig. 8

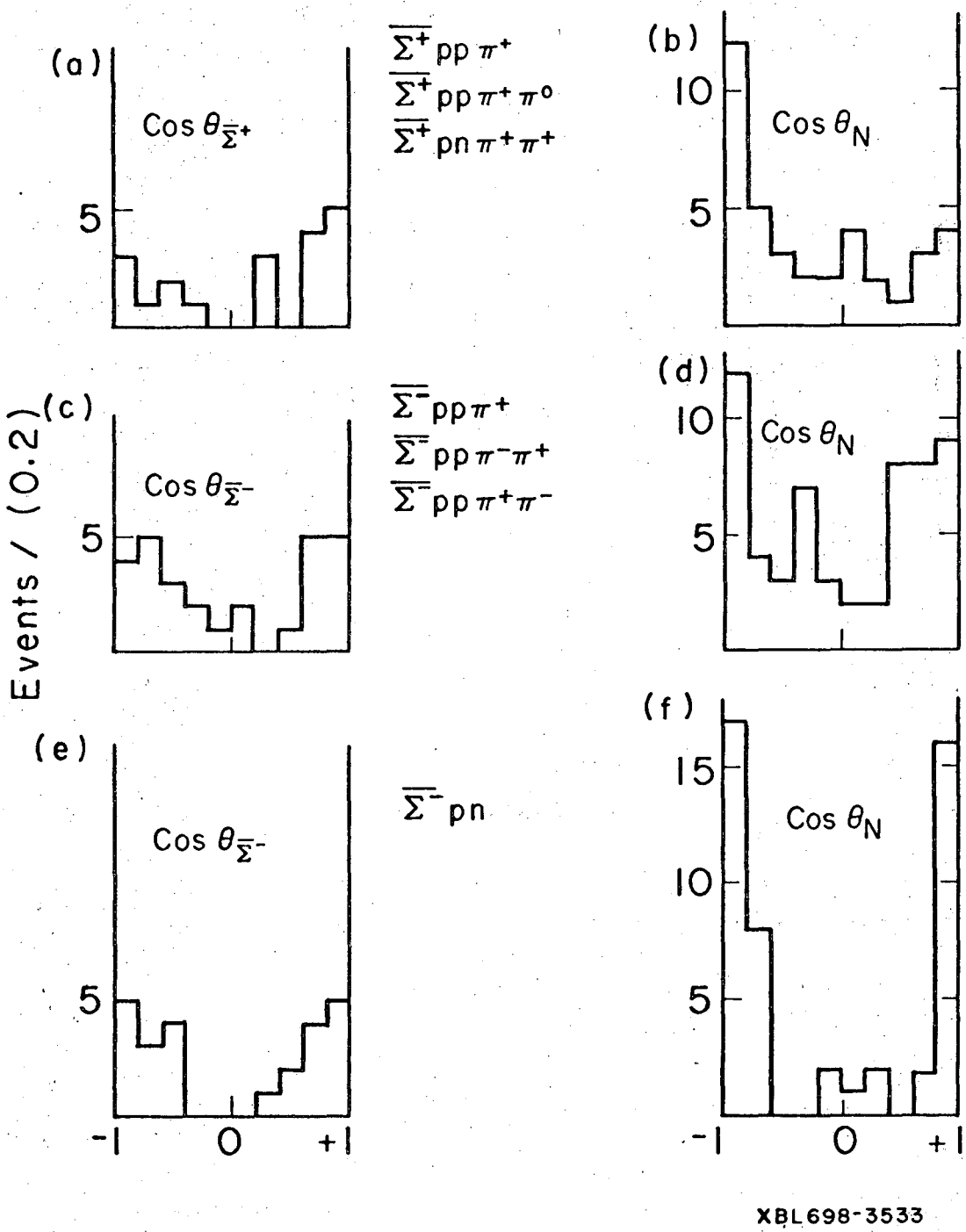
(a)
Cos $\theta_{\bar{\Sigma}^+}$
$\overline{\Sigma^+}$ pp π^+
$\overline{\Sigma^+}$ pp $\pi^+\pi^o$
$\overline{\Sigma^+}$ pn $\pi^+\pi^+$
(b)
Cos θ_N
(c)
Cos $\theta_{\bar{\Sigma}^-}$
$\overline{\Sigma^-}$ pp π^+
$\overline{\Sigma^-}$ pp $\pi^-\pi^+$
$\overline{\Sigma^-}$ pp $\pi^+\pi^-$
(d)
Cos θ_N
Events / (0.2)
(e)
Cos $\theta_{\bar{\Sigma}^-}$
$\overline{\Sigma^-}$ pn
(f)
Cos θ_N
XBL698-3533

Fig. 9

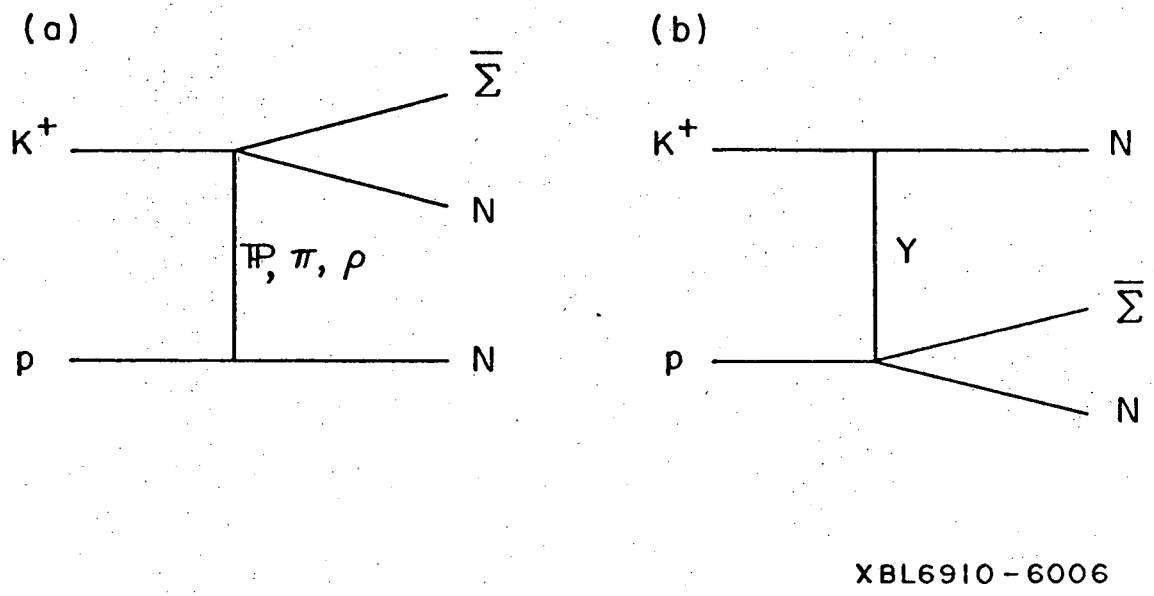
(a)
K^+
p
$\overline{\Sigma}$
N
N
$\mathbb{P}, \pi, \rho$
(b)
K^+
p
N
Y
$\overline{\Sigma}$
N
XBL6910-6006

Fig. 10

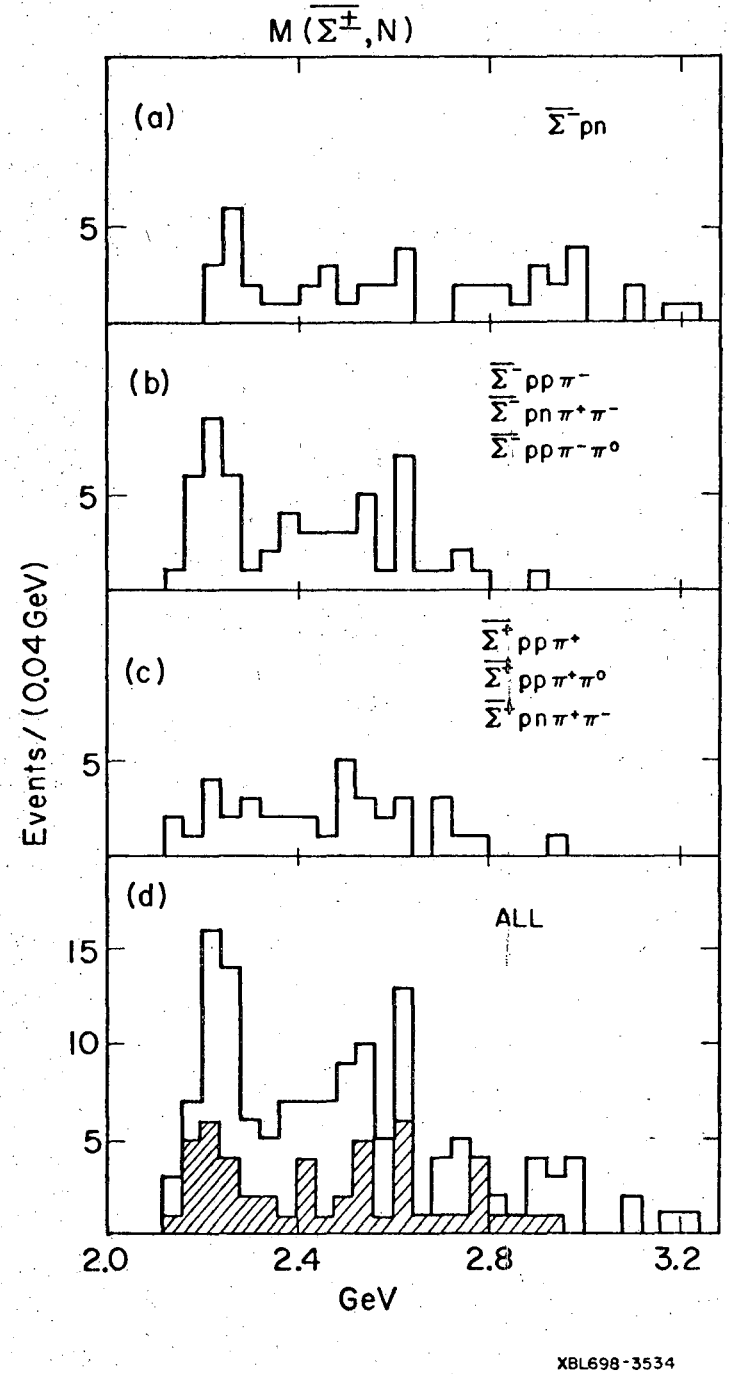
M($\overline{\Sigma^{\pm}}$,N)
(a)
$\overline{\Sigma^-}$pn
(b)
$\overline{\Sigma^-}$ppπ^-
$\overline{\Sigma^-}$pn$\pi^+\pi^-$
$\overline{\Sigma^-}$pp$\pi^-\pi^0$
(c)
$\overline{\Sigma^+}$ppπ^+
$\overline{\Sigma^+}$pp$\pi^+\pi^0$
$\overline{\Sigma^+}$pn$\pi^+\pi^-$
(d)
ALL
Events / (0.04 GeV)
5
5
5
15
10
5
2.0
2.4
2.8
3.2
GeV
XBL698-3534

Fig. 11

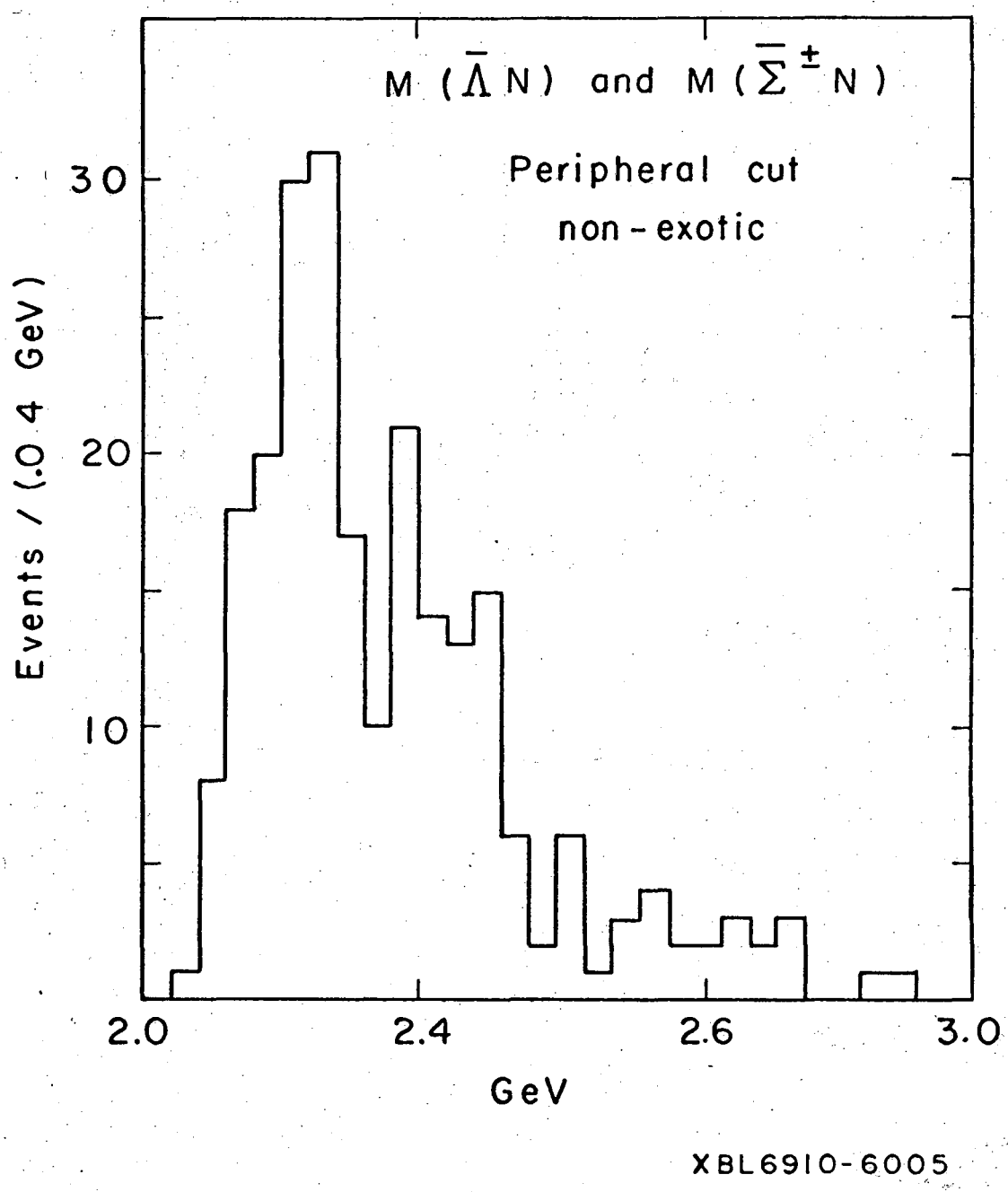
M ($\bar{\Lambda}$ N) and M ($\bar{\Sigma}^{\pm}$ N)
Peripheral cut
non-exotic
Events / (.04 GeV)
30
20
10
2.0
2.4
2.6
3.0
GeV
XBL6910-6005

Fig. 12

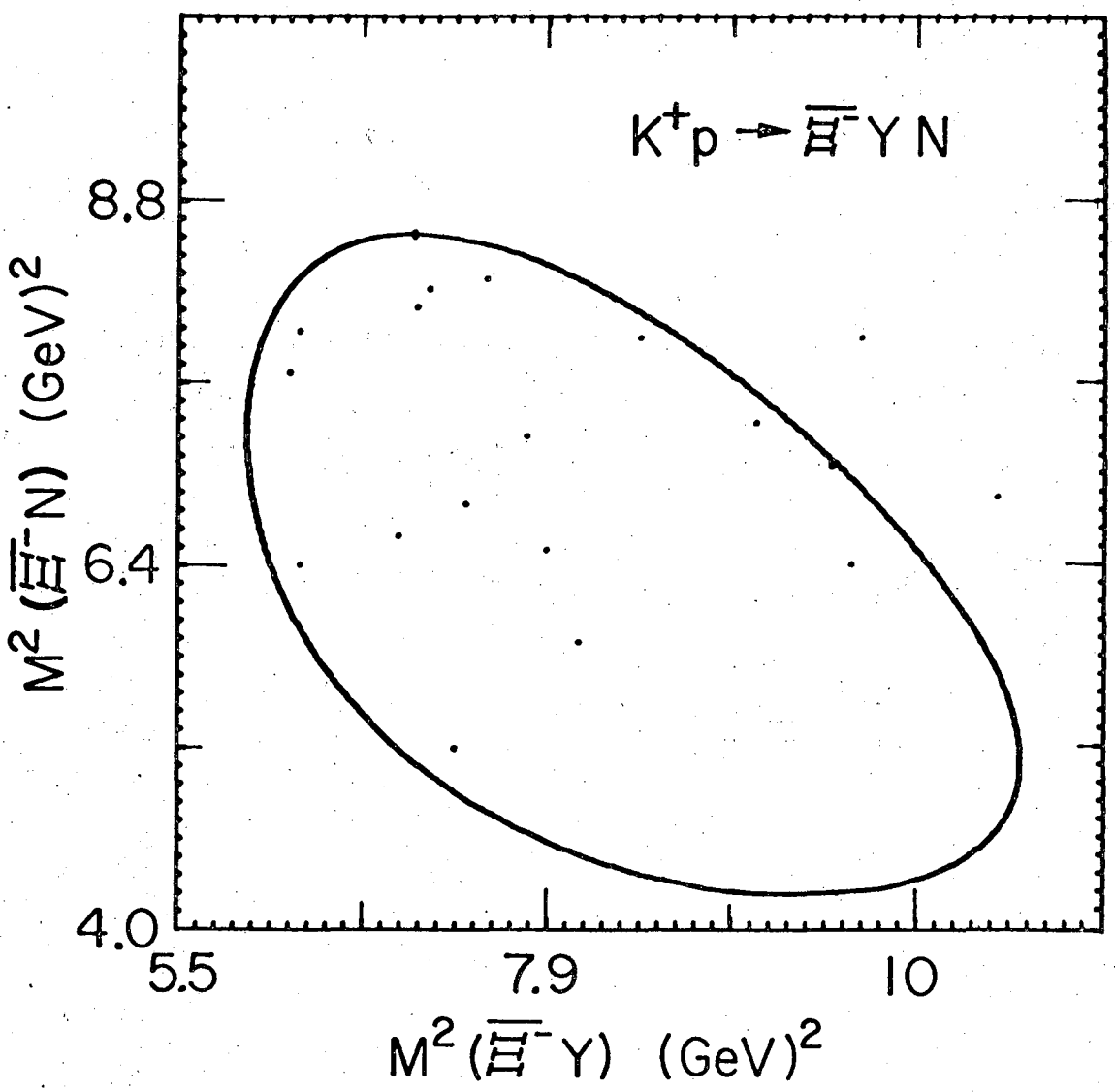

XBL698-3532

Fig. 13

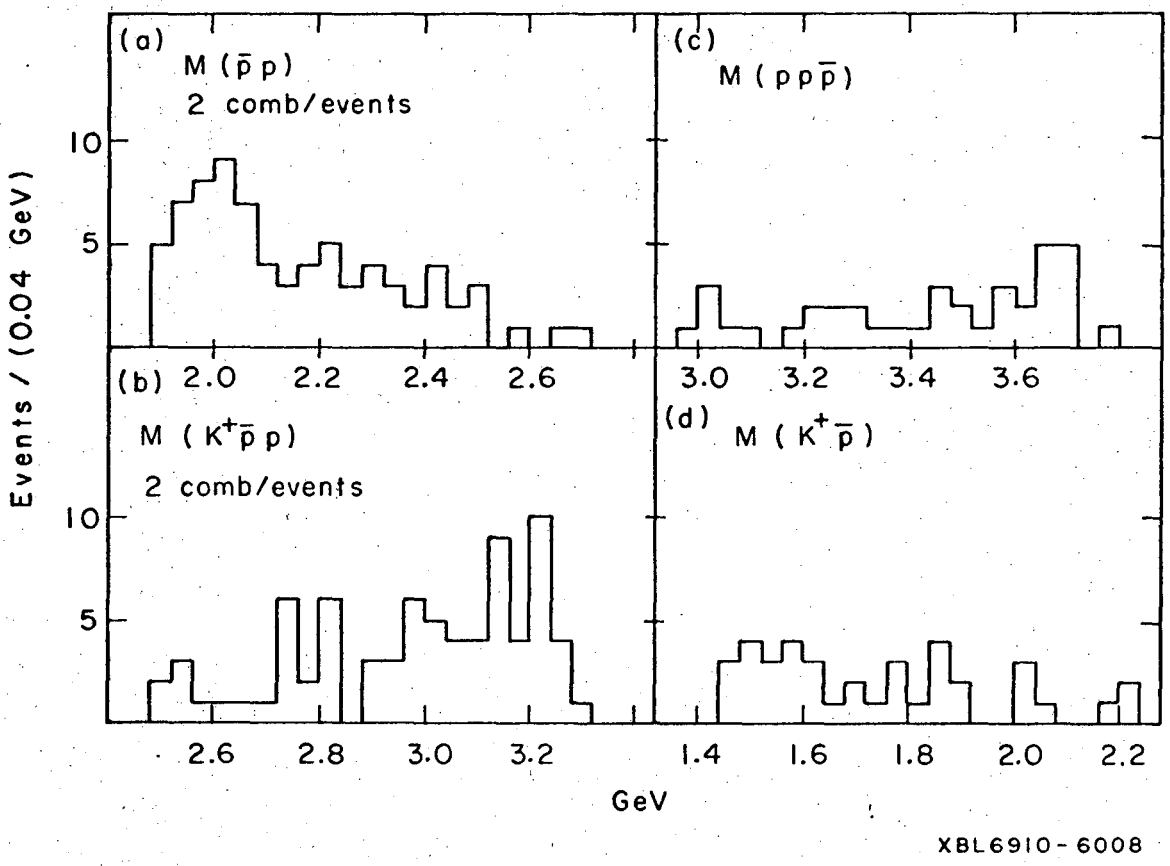
(a)
M ($\bar{p}$ p)
2 comb/events
(b)
M ($K^+\bar{p}$ p)
2 comb/events
(c)
M (p p $\bar{p}$)
(d)
M ($K^+\bar{p}$)
Events / (0.04 GeV)
10
5
2.0
2.2
2.4
2.6
3.0
3.2
3.4
3.6
2.6
2.8
3.0
3.2
1.4
1.6
1.8
2.0
2.2
GeV
XBL6910-6008

Fig. 14

TECHNICAL INFORMATION DIVISION
LAWRENCE RADIATION LABORATORY
UNIVERSITY OF CALIFORNIA
BERKELEY, CALIFORNIA 94720